


Realizing tunable higher-order topological superconductors with altermagnets

Yu-Xuan Li 

Centre for Quantum Physics, Key Laboratory of Advanced Optoelectronic Quantum Architecture and Measurement (MOE), School of Physics, *Beijing Institute of Technology*, Beijing 100081, China



(Received 10 March 2024; revised 15 May 2024; accepted 17 May 2024; published 4 June 2024)

We propose a method for realizing tunable higher-order topological superconductors (TSCs) by coupling class DIII TSCs with recently discovered altermagnets exhibiting nonrelativistic spin splitting. We exemplify our approach using d -wave spin splitting and demonstrate the emergence of inversion-protected Majorana zero modes (MZMs) localized at the corner of the system, i.e., Majorana corner modes. Critically, we show that manipulating the Néel vector of the altermagnets enables control over the MZM distribution. This constitutes a crucial step towards achieving non-Abelian braiding of MZMs, a key ingredient for fault-tolerant topological quantum computation. Finally, we discuss a physical system that implements our proposal.

DOI: [10.1103/PhysRevB.109.224502](https://doi.org/10.1103/PhysRevB.109.224502)

I. INTRODUCTION

Majorana zero modes (MZMs), considered fundamental to topological quantum computation, are a class of quasiparticles characterized by non-Abelian statistical properties [1–5]. Topological superconductors (TSCs) have garnered significant interest due to their potential to host MZMs [6–8]. In seminal work [9], Kitaev proposed that MZMs form at the endpoints of one-dimensional (1D) p -wave superconductors. However, the experimental realization of MZMs is hindered by the rarity of natural p -wave superconductors. Nonetheless, researchers are developing alternative approaches to overcome this obstacle [6,7,10–13]. Two approaches have been proposed to create MZMs. The first approach exploits the spin-momentum-locked surface states of 3D topological insulators (TIs) and induces superconductivity through the proximity effect, leading to the formation of MZMs in vortices [10]. The second approach involves constructing a heterojunction between a superconductor and semiconductor nanowires with strong spin-orbit coupling and then applying a Zeeman field [14–17]. This configuration creates an equivalent Kitaev chain, enabling the generation of MZMs.

Recently, there have been proposals for higher-order topological states that go beyond the traditional understanding of the bulk-boundary correspondence [18–48]. Rather than surface or edge states, these states involve topologically non-trivial hinge or corner states in 3D or 2D systems [44]. For example, in 2D second-order TSCs, MZMs may appear at the corners of the system, i.e., Majorana corner modes (MCMs). Several proposals have been made for the existence of MZMs in higher-order TSCs, such as the introduction of electron pairing in 2D TIs [29,30,38], creating π junctions between double-layer Rashba structures [35], applying Zeeman fields in 2D p -wave superconductors [31], and the use of twisted systems [47,48]. Experimental evidence for higher-order TSCs has also been observed [34]. However, there is still a lack of effective control schemes for MCMs in this field, which is crucial for achieving non-Abelian braiding of MZMs [1].

In the field of compensated magnetic materials, an important discovery has been made that involves a unique magnetic order known as altermagnetism (AM) [49–67]. The uniqueness of AM, in contrast to common ferromagnetism and antiferromagnetism, lies in its momentum-dependent spin splitting obeying nonrelativistic behavior [60], which has been experimentally verified [64,65,67]. This intriguing magnetic ordering is expected to produce many unique physical phenomena, including including Andreev reflection [57,58], the Josephson effect [56,63], and the existence of finite-momentum copper pairing [59,68]. The discovery of AM also opens up exciting prospects for the realisation of TSCs [55,62,66]. A natural question arises: Can altermagnets, with

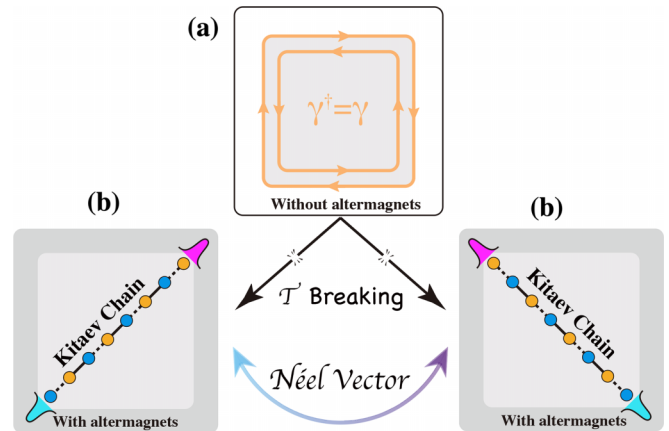


FIG. 1. (a) A 2D TRS TSC with helical edge states (orange-arrowed line) protected by time-reversal symmetry and particle-hole symmetry. (b) A proximitized altermagnet induces altermagnetism in the 2D TSC and breaks time-reversal symmetry. When the Néel vector is oriented around the [11] direction, the helical edge states create a gap with two MZMs localized at the corners, i.e., the MCMs. The manipulation of these MCMs can be achieved by adjusting the Néel vector, as indicated by the arrow. The MCMs marked in different colors indicate that they come from different mirror subspaces.

their nonrelativistic spin splitting and zero net magnetization, be used to manipulate MZMs?

In this paper, we give an answer in the affirmative. Specifically, we focus on 2D TSCs with time-reversal symmetry (TRS) and particle-hole symmetry (PHS), which belong to the class DIII [69]. As shown in Fig. 1(a), the system has helical edge states which are secured by TRS and PHS. When 2D TSCs are combined with altermagnets, the absence of net magnetization in the altermagnets still leads to the breaking of the TRS. As a result, the gapless helical edge states develop an energy gap, causing the system to exhibit a trivial first-order topological phase. However, we show that the appearance of MZMs at the corners of the system indicates a nontrivial second-order topology of the system.

Based on edge theory and symmetry analysis, our investigation has shown that when the Néel vector of the altermagnets is aligned along the [11] direction, the system has localized MZMs at the two corners along the $[1\bar{1}]$ direction, which can be likened to a one-dimensional Kitaev chain [9]. Additionally, as shown in Fig. 1(b), the position of the MZMs can be changed by rotating the Néel vector. These findings not only demonstrate the potential of altermagnets for the manipulation of topological quantum states, but also provide another way to realize non-Abelian statistics of MZMs. Last but not least, this discovery opens up potential applications for the recently discovered altermagnets.

II. MODEL

In order to determine the effect of altermagnets on the boundary state of class DIII topological superconductors, 2D $p \pm ip$ superconductors were selected here. The Bogoliubov-de Gennes (BdG) Hamiltonian for a 2D $p \pm ip$ superconductor is $\hat{H} = \frac{1}{2} \sum_{\mathbf{k}} \Psi_{\mathbf{k}}^{\dagger} \mathcal{H}(\mathbf{k}) \Psi_{\mathbf{k}}$ with $\Psi_{\mathbf{k}} = (c_{\mathbf{k},\uparrow}, c_{\mathbf{k},\downarrow}, c_{-\mathbf{k},\downarrow}^{\dagger}, -c_{-\mathbf{k},\uparrow}^{\dagger})$ and

$$\mathcal{H}(\mathbf{k}) = \epsilon(\mathbf{k})\tau_z - 2\Delta_0(\sin k_x s_x - \sin k_y s_y)\tau_x, \quad (1)$$

where $\epsilon(\mathbf{k}) = (\mu - 2t_x \cos k_x - 2t_y \cos k_y)$ is kinetic energy, and τ_i and s_j are Pauli matrices acting on the particle-hole and spin (\uparrow, \downarrow) degree of freedom, respectively. The 2D $p \pm ip$ superconductors have TRS $\mathcal{T} = i\tau_0 s_y \mathcal{K}$, chiral symmetry $\mathcal{C} = \tau_x s_z$, and PHS $\mathcal{P} = \tau_y s_y \mathcal{K}$, where \mathcal{K} is the complex conjugation. For gapped odd-parity superconductors in both 2D and 3D, their topological properties are determined by both the pairing nodes and the Fermi surfaces in the normal state [70,71]. Nontrivial topological superconductors can be identified by an odd number of Fermi surfaces enclosing the time-reversal invariant momentum (without considering the Kramers degeneracy for time-reversal invariant systems). Therefore, if the condition $\mu^2 - (2t_x + 2t_y)^2 < 0$ is satisfied, the $p \pm ip$ superconductors have a topologically invariant $\mathbb{Z}_2 = 1$. There are Majorana edge states protected by TRS and PHS, as shown by the blue dashed line in Fig. 2(a).

The altermagnets exhibit spin splitting of opposite sign in different regions of the Brillouin zone (BZ) [53]. For the purpose of demonstration, we focus in this work on the d -wave spin splitting, expressed in momentum space as

$$\mathcal{H}_{\text{AM}}(\mathbf{k}) = 2J_0(\cos k_x - \cos k_y)\mathbf{s} \cdot \hat{\mathbf{n}}, \quad (2)$$

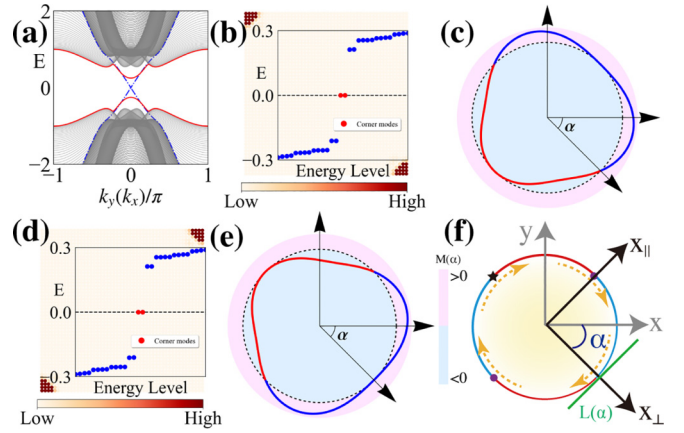


FIG. 2. (a) The edge spectrum for a cylinder geometry. The blue dotted lines represent the helical Majorana edge states of the $p \pm ip$ superconductors. The red solid lines denote the gapped Majorana edge states after the altermagnets are included. (b) Inset: Two in-gap states emerge with the Néel vector along the [11] direction. The real spatial distribution of their wave function is plotted. (d) Same as (b) except the Néel vector along the $[1\bar{1}]$ direction. (c), (e) The boundary Dirac mass changes with the rotation angle α when the Néel vector is along the [11] direction and the $[1\bar{1}]$ direction, respectively. The mass terms in the blue and magenta areas have opposite signs. (f) The tangents $L(\alpha)$, on which we will develop the generic edge theory, mark different boundaries with the clockwise rotation angle α . Common parameters: $\mu = 3.0$, $t_x = t_y = 1.0$, $\Delta_0 = 1.0$, $J_0 = 0.5$.

where $\hat{\mathbf{n}} = (\sin \theta \cos \varphi, \sin \theta \sin \varphi, \cos \theta)$ represents the direction of the Néel vector, and J_0 indicates the strength of spin splitting in BZ. Our current research focuses on the in-plane Néel component ($\theta = \pi/2$), and the out-of-plane component is discussed in the Supplemental Material (SM) [72]. We have calculated the energy spectrum of the cylinder geometry when the Néel vector is along the [11] direction and is represented by the red solid line in Fig. 2(a). It is observed that the incorporation of altermagnets into the $p \pm ip$ superconductor leads to gapped edge states and the system exhibits a trivial first-order topology. Instead, the energy spectrum of a finite-size system is calculated as shown in the inset of Fig. 2(b). There are two zero-energy states in the boundary gap. By analyzing the spatial distribution of the wave function corresponding to these two zero-energy states, we observe that they are localized at the two corners along the $[1\bar{1}]$ direction, as shown in Fig. 2(b). Although the altermagnetism renders the first-order topology trivial, the localization of the zero-energy states suggests that the system has a nontrivial second-order topology. Therefore, the altermagnets induce a phase transition at the boundary, driving the system from a first-order topological phase to a second-order topological phase [73].

The effect of rotating the in-plane Néel vector on the MZMs is then investigated. As the Néel vector deviates from the [11] direction, the localized length of the MZMs becomes anisotropic along the x and y directions. When the Néel vector aligns with the [10] direction ($\varphi = 0$), the cylinder system has gapless edge states along y , but has gapped edge states along the x direction. These results are consistent with our calculations of finite-sized structures in real space, which

confirm the presence of edge states along the x boundary [72]. Interestingly, aligning the Néel vector along the $[1\bar{1}]$ direction ($\varphi = -\pi/4$) reveals the reappearance of MCMs in Fig. 2(c), but localized at the corners along the $[11]$ direction. These observations demonstrate the emergence of a second-order TSCs phase and highlight the possibility of manipulating MCMs by controlling the Néel vector orientation. Experimental techniques, such as applying an electric field or a spin-orbit torque [74–76], can effectively modify and reposition the Néel vector.

III. EDGE THEORY

To elucidate the relationship between the Néel vector's azimuthal orientation and MCM localization, we now turn to edge theory. The BdG Hamiltonian for 2D second-order TSCs is $\mathcal{H}^{\text{BdG}}(\mathbf{k}) = \mathcal{H}(\mathbf{k}) + \mathcal{H}_{\text{AM}}(\mathbf{k})$. Expanding the Hamiltonian $\mathcal{H}^{\text{BdG}}(\mathbf{k})$ at the band inversion point $\Gamma = (0, 0)$ to the second order, we obtain

$$\begin{aligned} \mathcal{H}^{\text{eff}}(\mathbf{k}) = & (m + t_x k_x^2 + t_y k_y^2) \tau_z - 2\Delta_0 k_x s_x \tau_x \\ & + 2\Delta_0 k_y s_y \tau_y - J_0 (k_x^2 - k_y^2) \mathbf{s} \cdot \hat{\mathbf{n}}, \end{aligned} \quad (3)$$

where $m = \mu - 2t_x - 2t_y$. The edge terminations in a 2D system can be represented as tangent lines to the unit circle [19,77], as shown in Fig. 2(f). To visualize the anisotropy of the boundary Dirac mass originating from altermagnets, by rotating the coordinate system clockwise by an angle α , we can analyze the dispersion of the arbitrary tangential boundary $L(\alpha)$. The transformation relating the rotated and original coordinate systems is expressed as

$$\begin{pmatrix} k_x \\ k_y \end{pmatrix} = \begin{pmatrix} \cos \alpha & -\sin \alpha \\ \sin \alpha & \cos \alpha \end{pmatrix} \begin{pmatrix} k_{\perp} \\ k_{\parallel} \end{pmatrix}. \quad (4)$$

For the rotated coordinate system, under the condition that the strength of the altermagnetism is smaller than the bulk gap of the TSCs, the Hamiltonian can be decomposed into $\mathcal{H}^{\text{eff}}(k_{\perp}, k_{\parallel}) = \mathcal{H}_0 + \mathcal{H}_p$ (see details in SM [72]). Consider a semi-infinite plane $x_{\perp} \in (-\infty, 0]$ with a boundary at $x_{\perp} = 0$, where the momentum k_{\perp} is replaced by $-i\partial_{\perp}$. We solve the eigenequation $H_0 \psi_{\alpha}(x_{\perp}) = E_{\alpha} \psi_{\alpha}(x_{\perp})$ with the boundary condition $\psi_{\alpha}(0) = \psi_{\alpha}(-\infty) = 0$. For $E_{\alpha} = 0$, two solutions can be obtained as $\psi_{\alpha}(x_{\perp}) = \mathcal{N}_{\perp} \sin(\kappa_1 x_{\perp}) e^{i\kappa_2 x_{\perp}} e^{ik_{\parallel} x_{\parallel}} \chi_{\alpha}$, where the normalization constant is given by $|\mathcal{N}_{\perp}|^2 = 4|\kappa_2(\kappa_1^2 + \kappa_2^2)/\kappa_1^2|$. The eigenvector ξ_{α} satisfies $(\sin \alpha s_x + \cos \alpha s_y) \tau_y \xi_{\alpha} = \xi_{\alpha}$. We choose ξ_i as $\xi_1 = 1/\sqrt{2}(-e^{i\alpha}, 0, 0, 1)^T$ and $\xi_2 = 1/\sqrt{2}(0, e^{i\alpha}, 1, 0)^T$. Upon projecting the perturbation term \mathcal{H}_p onto the basis ψ_1, ψ_2 , we obtain

$$\mathcal{H}_{\text{edge}}(x_{\perp}, k_{\parallel}) = 2\Delta_0 k_{\parallel} \eta_z + M(\alpha, \theta, \varphi) \eta_y, \quad (5)$$

the Dirac mass induced by the altermagnets read as

$$M(\alpha, \theta, \varphi) \sim \sin \theta \cos(2\alpha)(\cos \varphi \sin \alpha + \sin \varphi \cos \alpha). \quad (6)$$

Equation (6) reveals that the Dirac mass depends on both the azimuthal angle φ and the polar angle θ of the Néel vector, along with the edge direction α . Intriguingly, the boundary states of 2D $p \pm ip$ superconductors are also protected by an additional mirror symmetry \mathcal{M}_z . As a result, the out-of-plane component ($\theta = 0$) of the Néel vector does not affect

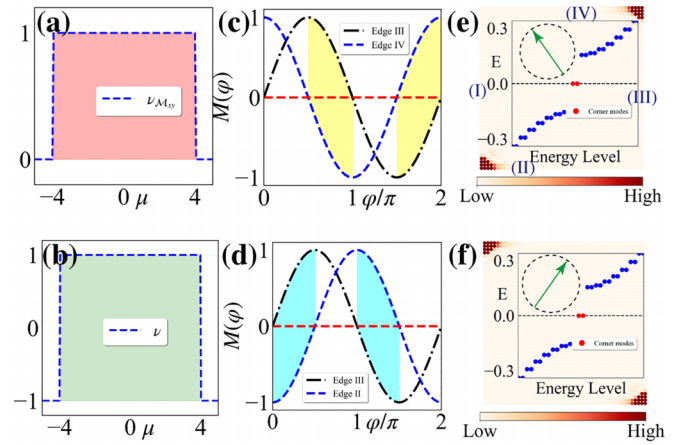


FIG. 3. (a) The mirror-graded winding number is plotted as a function of the chemical potential μ . The presence of MCMs is indicated by the light red area in the plot. (b) The Pfaffian is shown to vary with the chemical potential, where the light green region indicates that the 1D Kitaev chain is in a nontrivial phase. (c) The Dirac masses of boundaries III and IV are displayed as a function of the azimuth angle φ . (d) The Dirac masses of boundaries III and II are plotted. (e) Inset: Two in-gap states emerge with the azimuth of Néel vector is $\varphi = 0.7\pi$. The real spatial distribution of their wave function is plotted. (f) Same as (e) except the azimuth of Néel vector is $\varphi = 0.3\pi$. Common parameters: $\mu = 3.0$, $t_x = t_y = 1.0$, $\Delta_0 = 1.0$, $J_0 = 0.5$.

the boundary states [72]. In Fig. 2(e), we plot the variation of the Dirac mass with respect to the boundary direction α for the case where the Néel vector aligns along the $[1\bar{1}]$ direction. We find that the Dirac mass undergoes a sign reversal at specific angles, such as $\alpha = 3\pi/4$ and $\alpha = 7\pi/4$. This sign reversal leads to the formation of bound states that are akin to the Jackiw-Rebbi mode [78]. Likewise, for the Néel vector oriented along the $[11]$ direction, the Dirac mass exhibits dependence on the boundary direction α , as shown in Fig. 2(b). This behavior is consistent with the emergence of mass domain walls observed numerically at $\alpha = \pi/4$ and $\alpha = 5\pi/4$ in Fig. 2(c).

Building upon the connection between MCMs and the Néel vector's azimuthal angle (φ) established by edge theory, our results demonstrate that MCMs can propagate along the boundary as φ is varied [72]. This finding paves the way for the precise manipulation of MCMs in experiments through controlled manipulation of the Néel vector orientation [75,79,80].

IV. TOPOLOGICAL INVARIANT

To gain a deeper understanding, we focus on the inversion symmetry $\mathcal{I} = \tau_z \sigma_0$ of the system. This symmetry remains intact when the altermagnet strength is weak and the band order is preserved. This preserved inversion symmetry with a \mathbb{Z}_2 classification protects the MCMs [28], allowing them to appear in pairs at the corners of inversion-related domains. To facilitate the discussion, we consider a square geometry where each edge is labeled I, II, III, and IV, as shown in Fig. 3(e). According to edge theory, the boundary Dirac mass is plotted as a variation of the azimuthal angle φ of the Néel vector,

Eq. (6), as shown in Figs. 3(c) and 3(d). In the colored region, it is clear that the Dirac mass at the adjacent boundaries has an opposite sign, resulting in the formation of a mass domain. As a result, each mass domain wall is associated with an MCM. A specific set of azimuthal angles, namely $\varphi = 0.3\pi$ and $\varphi = 0.7\pi$, were used to compute the energy spectrum of the finite-size system. The energy spectrum is shown in Figs. 3(e) and 3(f). Within the boundary gap, two zero-energy bound states emerge, with their wave functions centered at the inversion-related corners.

Interestingly, when the Néel vector is along the [11] direction, the Hamiltonian $\mathcal{H}^{\text{BdG}}(\mathbf{k})$ exhibits an additional reflection symmetry $\mathcal{M}_{xy} = i\sqrt{2}/2(s_x - s_y)$, which transforms the coordinate (k_x, k_y) into $(-k_y, -k_x)$. One can decompose $\mathcal{H}^{\text{BdG}}(\mathbf{k})$ into different mirror subspaces at the reflection invariant line $k_x = -k_y$ based on the mirror eigenvalues $\pm i$,

$$\mathcal{H}^{\pm i}(k) = -(\mu - 4t \cos k)\eta_z \pm 4\Delta_0 \sin k\eta_x, \quad (7)$$

where η_i are Pauli matrices that act on mirror eigenvectors. In each mirror subspace, the Hamiltonian can be expressed as $\mathcal{H}^{\pm i} = \mathbf{q}_{\pm i}(k) \cdot \boldsymbol{\eta}$, the computed winding numbers are ν_{+i} and ν_{-i} , respectively. Thus, the mirror-graded winding number is calculated by $\nu_{\mathcal{M}_{xy}} = (\nu_{+i} - \nu_{-i})/2$ with

$$\nu_{\pm i} = \frac{i}{2\pi} \int_L dk \{ \text{Tr}[\mathbf{q}_{\pm i}(k) \partial_k \mathbf{q}_{\pm i}^*(k)] \}. \quad (8)$$

Our calculations of the mirror-graded winding number $\nu_{\mathcal{M}_{xy}}$, shown in Fig. 3(a), reveal a nonzero value for chemical potentials within $\mu \in (-4, 4)$. This signifies that the system belongs to the class of second-order topological superconductors (TSCs) characterized by the presence of in-gap corner states [81]. Furthermore, when the Néel vector aligns along the $[1\bar{1}]$ direction, the reflection symmetry $\mathcal{M}_{x\bar{y}} = i\sqrt{2}/2(s_x + s_y)$ maps momenta (k_x, k_y) to (k_y, k_x) . Similar to the [11] case, the existence of MCMs is confirmed by a nonzero mirror-graded winding number $\nu_{\mathcal{M}_{x\bar{y}}}$ [72]. Through the implementation of the unitary operation $U = e^{i\pi/4\eta_z}$, each Hamiltonian in the mirror subspace reads

$$\mathcal{H}^{\pm i}(k) = -(\mu - 4t \cos k)\eta_z \pm 4\Delta_0 \sin k\eta_y. \quad (9)$$

Notably, the Hamiltonian of each subspace becomes a one-dimensional Kitaev chain [9]. This one-dimensional Kitaev chain can be conveniently expressed in the Majorana basis, expressed as

$$\mathcal{H}^{\pm i} = \frac{i}{4} \sum_k \psi_k^\dagger \mathcal{A}^{\pm i}(k) \psi_k, \quad (10)$$

where $\psi_k^T = (\gamma_{1,-k}, \gamma_{2,-k})$ and

$$\mathcal{A}^{\pm i}(k) = \begin{pmatrix} 0 & \zeta^{\pm i}(k) \\ -\zeta^{\pm i*}(k) & 0 \end{pmatrix}, \quad (11)$$

where the off-diagonal elements are $\zeta^{\pm i}(k) = -\mu + 4t \cos k \pm 4i\Delta_0 \sin k$. A topological phase transition occurs when the determinant of $\mathcal{A}^{\pm i}(k)$ is equal to zero. Notably, in more general cases, the matrix $\mathcal{A}^{\pm i}(k)$ can also be off diagonal. At two time-reversal invariant momentum points $k = 0, \pi$ the matrix $\mathcal{A}^{\pm i}(k)$ is antisymmetric, allowing us to define the Pfaffian [9]. Evaluating the Pfaffian of $\mathcal{A}(k)$ at time-reversal invariant momentum points ($k = 0, \pi$), one can

determine the topological invariant

$$\begin{aligned} (-1)^\nu &= \text{sgn}[\text{Pf}[\mathcal{A}(k=0)]] \text{sgn}[\text{Pf}[\mathcal{A}(k=\pi)]] \\ &= \text{sgn}[-4t - \mu] \text{sgn}[4t - \mu]. \end{aligned} \quad (12)$$

The Kitaev chain exhibits a nontrivial phase characterized by a topological invariant $\nu = 1$ when $|\mu| < 4t$. In this nontrivial phase, the system harbors MZMs localized at the endpoints of the chain. Conversely, the system transitions to a trivial phase with $\nu = -1$ for $|\mu| > 4t$. This behavior of the topological invariant ν is depicted in Fig. 3(b). Therefore, if the Néel vector is aligned along either the [11] or $[1\bar{1}]$ direction, the system can be viewed as a 1D Kitaev chain in each mirror space. Intuitively, two nontrivial Kitaev chains will contribute four end states. However, when the Néel vector deviates from the [11] ($[1\bar{1}]$) direction, the mirror symmetry \mathcal{M}_{xy} ($\mathcal{M}_{x\bar{y}}$) of the system is broken, and the gap closure does not occur. Consequently, the system remains in a topological phase with a \mathbb{Z}_2 classification [22,28]. Furthermore, the lack of TRS means that there can only be one stable MCM per corner. As a result, when the Néel vector is in the [11] ($[1\bar{1}]$) direction, there are only two MCMs in the system instead of four. Interestingly, despite the introduction of altermagnets in $p \pm ip$ superconductors and absence of TRS, the system still possesses chiral symmetry \mathcal{C} , and it satisfies

$$\{M_{xy}(\mathcal{M}_{x\bar{y}}), \mathcal{C}\} = 0. \quad (13)$$

According to Eq. (13) it can be concluded that the two MZMs at the corners belong to different mirror subspaces. Therefore, although the system is equivalent to 1D Kitaev in each mirror subspace, chiral symmetry ensures that the MZMs at each corner come from different mirror subspaces, as shown in Fig. 1(b) marked by different colors.

V. DISCUSSIONS AND CONCLUSIONS

Our work demonstrates the creation of tunable second-order TSCs with MCMs by combining a recently discovered altermagnet with a first-order TSC possessing TRS. Crucially, by controlling the Néel vector of the altermagnet, we can manipulate the MCM distribution. This ability to manipulate the MCMs highlights their topological nature and potential for applications in topological quantum computing and related fields. Furthermore, experimental techniques established for antiferromagnetic materials, such as current, voltage manipulation [75,79], and spin-orbit torques [80], offer promising avenues for practical applications. These techniques enable effective control and detection of the Néel vector orientation. Additionally, the antiferromagnet's inherent robustness against external magnetic fields and ultrafast response due to the absence of a coercive field [82] make them particularly attractive for braiding MZMs.

Candidates for the realization of the time-reversal symmetry TSC include a bilayer Rashba with an interlayer interaction [83] and an s -wave superconducting Josephson junction with a phase difference $\phi = \pi$ [84], a doped quantum spin Hall insulator [85], and n -type doped BiH [86]. The low-energy physics of the above systems can be described as superconductors with $p \pm ip$ pairings. We expect that the introduction of altermagnets into these systems can lead to second-order topological superconductors with tunable corner states.

ACKNOWLEDGMENTS

It is our pleasure to thank Jinyi Duan and Bing-Bing Wang for their insightful discussions. The work is sup-

ported by the National Key & Program of China (Grant No. 2020YFA0308800), the NSF of China (Grant No. 12374055), and the Science Fund for Creative Research Groups of NSFC (Grant No. 12321004).

- [1] A. Yu. Kitaev, *Ann. Phys.* **303**, 2 (2003).
- [2] J. Alicea, Y. Oreg, G. Refael, F. von Oppen, and M. P. A. Fisher, *Nat. Phys.* **7**, 412 (2011).
- [3] C. Beenakker, *Annu. Rev. Condens. Matter Phys.* **4**, 113 (2013).
- [4] S. R. Elliott and M. Franz, *Rev. Mod. Phys.* **87**, 137 (2015).
- [5] S. D. Sarma, M. Freedman, and C. Nayak, *npj Quantum Inf.* **1**, 15001 (2015).
- [6] X.-L. Qi and S.-C. Zhang, *Rev. Mod. Phys.* **83**, 1057 (2011).
- [7] J. Alicea, *Rep. Prog. Phys.* **75**, 076501 (2012).
- [8] M. Sato and S. Fujimoto, *J. Phys. Soc. Jpn.* **85**, 072001 (2016).
- [9] A. Y. Kitaev, *Phys. Usp.* **44**, 131 (2001).
- [10] L. Fu and C. L. Kane, *Phys. Rev. Lett.* **100**, 096407 (2008).
- [11] R. M. Lutchyn, J. D. Sau, and S. Das Sarma, *Phys. Rev. Lett.* **105**, 077001 (2010).
- [12] Y. Oreg, G. Refael, and F. von Oppen, *Phys. Rev. Lett.* **105**, 177002 (2010).
- [13] J. D. Sau, R. M. Lutchyn, S. Tewari, and S. Das Sarma, *Phys. Rev. Lett.* **104**, 040502 (2010).
- [14] V. Mourik, K. Zuo, S. M. Frolov, S. R. Plissard, E. P. A. M. Bakkers, and L. P. Kouwenhoven, *Science* **336**, 1003 (2012).
- [15] D. Wang, L. Kong, P. Fan, H. Chen, S. Zhu, W. Liu, L. Cao, Y. Sun, S. Du, J. Schneeloch, R. Zhong, G. Gu, L. Fu, H. Ding, and H.-J. Gao, *Science* **362**, 333 (2018).
- [16] B. Jäck, Y. Xie, J. Li, S. Jeon, B. A. Bernevig, and A. Yazdani, *Science* **364**, 1255 (2019).
- [17] M. Li, G. Li, L. Cao, X. Zhou, X. Wang, C. Jin, C.-K. Chiu, S. J. Pennycook, Z. Wang, and H.-J. Gao, *Nature (London)* **606**, 890 (2022).
- [18] M. Sitte, A. Rosch, E. Altman, and L. Fritz, *Phys. Rev. Lett.* **108**, 126807 (2012).
- [19] F. Zhang, C. L. Kane, and E. J. Mele, *Phys. Rev. Lett.* **110**, 046404 (2013).
- [20] W. A. Benalcazar, B. A. Bernevig, and T. L. Hughes, *Science* **357**, 61 (2017).
- [21] F. Liu and K. Wakabayashi, *Phys. Rev. Lett.* **118**, 076803 (2017).
- [22] J. Langbehn, Y. Peng, L. Trifunovic, F. von Oppen, and P. W. Brouwer, *Phys. Rev. Lett.* **119**, 246401 (2017).
- [23] Z. Song, Z. Fang, and C. Fang, *Phys. Rev. Lett.* **119**, 246402 (2017).
- [24] M. Ezawa, *Phys. Rev. Lett.* **120**, 026801 (2018).
- [25] F. Schindler, Z. Wang, M. G. Vergniory, A. M. Cook, A. Murani, S. Sengupta, A. Y. Kasumov, R. Deblock, S. Jeon, I. Drozdov, H. Bouchiat, S. Guéron, A. Yazdani, B. A. Bernevig, and T. Neupert, *Nat. Phys.* **14**, 918 (2018).
- [26] F. Schindler, A. M. Cook, M. G. Vergniory, Z. Wang, S. S. P. Parkin, B. A. Bernevig, and T. Neupert, *Sci. Adv.* **4**, eaat0346 (2018).
- [27] C.-H. Hsu, P. Stano, J. Klinovaja, and D. Loss, *Phys. Rev. Lett.* **121**, 196801 (2018).
- [28] E. Khalaf, *Phys. Rev. B* **97**, 205136 (2018).
- [29] Q. Wang, C.-C. Liu, Y.-M. Lu, and F. Zhang, *Phys. Rev. Lett.* **121**, 186801 (2018).
- [30] T. Liu, J. J. He, and F. Nori, *Phys. Rev. B* **98**, 245413 (2018).
- [31] X. Zhu, *Phys. Rev. B* **97**, 205134 (2018).
- [32] X.-H. Pan, K.-J. Yang, L. Chen, G. Xu, C.-X. Liu, and X. Liu, *Phys. Rev. Lett.* **123**, 156801 (2019).
- [33] Y. Peng and G. Refael, *Phys. Rev. Lett.* **123**, 016806 (2019).
- [34] M. J. Gray, J. Freudenstein, S. Y. F. Zhao, R. O'Connor, S. Jenkins, N. Kumar, M. Hoek, A. Kopec, S. Huh, T. Taniguchi, K. Watanabe, R. Zhong, C. Kim, G. D. Gu, and K. S. Burch, *Nano Lett.* **19**, 4890 (2019).
- [35] Y. Volpez, D. Loss, and J. Klinovaja, *Phys. Rev. Lett.* **122**, 126402 (2019).
- [36] Y. Xu, Z. Song, Z. Wang, H. Weng, and X. Dai, *Phys. Rev. Lett.* **122**, 256402 (2019).
- [37] W. A. Benalcazar, T. Li, and T. L. Hughes, *Phys. Rev. B* **99**, 245151 (2019).
- [38] Z. Yan, F. Song, and Z. Wang, *Phys. Rev. Lett.* **121**, 096803 (2018).
- [39] R.-X. Zhang, W. S. Cole, and S. Das Sarma, *Phys. Rev. Lett.* **122**, 187001 (2019).
- [40] X. Wu, W. A. Benalcazar, Y. Li, R. Thomale, C.-X. Liu, and J. Hu, *Phys. Rev. X* **10**, 041014 (2020).
- [41] R.-X. Zhang, J. D. Sau, and S. Das Sarma, *Phys. Rev. B* **108**, 115146 (2023).
- [42] Y. Ren, Z. Qiao, and Q. Niu, *Phys. Rev. Lett.* **124**, 166804 (2020).
- [43] Y.-J. Wu, J. Hou, Y.-M. Li, X.-W. Luo, X. Shi, and C. Zhang, *Phys. Rev. Lett.* **124**, 227001 (2020).
- [44] B. Xie, H.-X. Wang, X. Zhang, P. Zhan, J.-H. Jiang, M. Lu, and Y. Chen, *Nat. Rev. Phys.* **3**, 520 (2021).
- [45] L.-H. Hu and R.-X. Zhang, *arXiv:2207.10113*.
- [46] S. Qin, C. Fang, F.-C. Zhang, and J. Hu, *Phys. Rev. X* **12**, 011030 (2022).
- [47] A. Chew, Y. Wang, B. A. Bernevig, and Z.-D. Song, *Phys. Rev. B* **107**, 094512 (2023).
- [48] Y.-X. Li and C.-C. Liu, *Phys. Rev. B* **107**, 235125 (2023).
- [49] K.-H. Ahn, A. Hariki, K.-W. Lee, and J. Kuneš, *Phys. Rev. B* **99**, 184432 (2019).
- [50] L.-D. Yuan, Z. Wang, J.-W. Luo, E. I. Rashba, and A. Zunger, *Phys. Rev. B* **102**, 014422 (2020).
- [51] L. Šmejkal, R. González-Hernández, T. Jungwirth, and J. Sinova, *Sci. Adv.* **6**, eaaz8809 (2020).
- [52] H. Reichlová, R. L. Seeger, R. González-Hernández, I. Kounta, R. Schlitz, D. Kriegner, P. Ritzinger, M. Lammel, M. Leiviskä, V. Petříček, P. Doležal, E. Schmoranzarová, A. Bad'ura, A. Thomas, V. Baltz, L. Michez, J. Sinova, S. T. B. Goennenwein, T. Jungwirth, and L. Šmejkal, *arXiv:2012.15651*.
- [53] L. Šmejkal, J. Sinova, and T. Jungwirth, *Phys. Rev. X* **12**, 031042 (2022).
- [54] S. Das, D. Suri, and A. Soori, *J. Phys.: Condens. Matter* **35**, 435302 (2023).
- [55] S. A. A. Ghorashi, T. L. Hughes, and J. Cano, *arXiv:2306.09413*.

- [56] J. A. Ouassou, A. Brataas, and J. Linder, *Phys. Rev. Lett.* **131**, 076003 (2023).
- [57] M. Papaj, *Phys. Rev. B* **108**, L060508 (2023).
- [58] C. Sun, A. Brataas, and J. Linder, *Phys. Rev. B* **108**, 054511 (2023).
- [59] S.-B. Zhang, L.-H. Hu, and T. Neupert, *Nat. Commun.* **15**, 1801 (2024).
- [60] L. Šmejkal, J. Sinova, and T. Jungwirth, *Phys. Rev. X* **12**, 040501 (2022).
- [61] X. Zhou, W. Feng, R.-W. Zhang, L. Šmejkal, J. Sinova, Y. Mokrousov, and Y. Yao, *Phys. Rev. Lett.* **132**, 056701 (2024).
- [62] D. Zhu, Z.-Y. Zhuang, Z. Wu, and Z. Yan, *Phys. Rev. B* **108**, 184505 (2023).
- [63] C. W. J. Beenakker and T. Vakhel, *Phys. Rev. B* **108**, 075425 (2023).
- [64] T. Osumi, S. Souma, T. Aoyama, K. Yamauchi, A. Honma, K. Nakayama, T. Takahashi, K. Ohgushi, and T. Sato, *Phys. Rev. B* **109**, 115102 (2024).
- [65] Y.-P. Zhu, X. Chen, X.-R. Liu, Y. Liu, P. Liu, H. Zha, G. Qu, C. Hong, J. Li, Z. Jiang, X.-M. Ma, Y.-J. Hao, M.-Y. Zhu, W. Liu, M. Zeng, S. Jayaram, M. Lenger, J. Ding, S. Mo, K. Tanaka *et al.*, *Nature (London)* **626**, 523 (2024).
- [66] Y.-X. Li and C.-C. Liu, *Phys. Rev. B* **108**, 205410 (2023).
- [67] J. Krempaský, L. Šmejkal, S. W. D'Souza, M. Hajlaoui, G. Springholz, K. Uhlířová, F. Alarab, P. C. Constantinou, V. Strocov, D. Usanov, W. R. Pudelko, R. González-Hernández, A. Birk Hellenes, Z. Jansa, H. Reichlová, Z. Šobáň, R. D. Gonzalez Betancourt, P. Wadley, J. Sinova, D. Kriegner *et al.*, *Nature (London)* **626**, 517 (2024).
- [68] D. Chakraborty and A. M. Black-Schaffer, [arXiv:2309.14427](https://arxiv.org/abs/2309.14427).
- [69] A. P. Schnyder, S. Ryu, A. Furusaki, and A. W. W. Ludwig, *Phys. Rev. B* **78**, 195125 (2008).
- [70] L. Fu and E. Berg, *Phys. Rev. Lett.* **105**, 097001 (2010).
- [71] M. Sato, *Phys. Rev. B* **81**, 220504(R) (2010).
- [72] See Supplemental Material at <http://link.aps.org/supplemental/10.1103/PhysRevB.109.224502> for more detailed information on (I) the derivation of the edge Hamiltonian for the Néel vector along an arbitrary direction and the manipulation of the topological corner states by rotating the Néel vector, and (II) calculation of the mirror-graded winding number when the Néel vector is along the $[1\bar{1}]$ direction, which includes Refs. [1,2,19,77,78,81].
- [73] E. Khalaf, W. A. Benalcazar, T. L. Hughes, and R. Queiroz, *Phys. Rev. Res.* **3**, 013239 (2021).
- [74] M. Meinert, D. Graulich, and T. Matalla-Wagner, *Phys. Rev. Appl.* **9**, 064040 (2018).
- [75] J. Godinho, H. Reichlová, D. Kriegner, V. Novák, K. Olejník, Z. Kašpar, Z. Šobáň, P. Wadley, R. P. Campion, R. M. Otxoa, P. E. Roy, J. Železný, T. Jungwirth, and J. Wunderlich, *Nat. Commun.* **9**, 4686 (2018).
- [76] S. Yu. Bodnar, L. Šmejkal, I. Turek, T. Jungwirth, O. Gomonay, J. Sinova, A. A. Sapozhnik, H.-J. Elmers, M. Kläui, and M. Jourdan, *Nat. Commun.* **9**, 348 (2018).
- [77] F. Zhang, C. L. Kane, and E. J. Mele, *Phys. Rev. B* **86**, 081303(R) (2012).
- [78] R. Jackiw and C. Rebbi, *Phys. Rev. D* **13**, 3398 (1976).
- [79] A. Mahmood, W. Echtenkamp, M. Street, J.-L. Wang, S. Cao, T. Komesu, P. A. Dowben, P. Buragohain, H. Lu, A. Gruverman, A. Parthasarathy, S. Rakheja, and C. Binek, *Nat. Commun.* **12**, 1674 (2021).
- [80] P. Zhang, C.-T. Chou, H. Yun, B. C. McGoldrick, J. T. Hou, K. A. Mkhoyan, and L. Liu, *Phys. Rev. Lett.* **129**, 017203 (2022).
- [81] D. Bercioux, J. Cayssol, M. G. Vergniory, and M. Reyes Calvo, *Topological Matter: Lectures from the Topological Matter School* (Springer Nature, Switzerland AG, 2018), Chap. 2.3.
- [82] V. Baltz, A. Manchon, M. Tsoi, T. Moriyama, T. Ono, and Y. Tserkovnyak, *Rev. Mod. Phys.* **90**, 015005 (2018).
- [83] S. Nakosai, Y. Tanaka, and N. Nagaosa, *Phys. Rev. Lett.* **108**, 147003 (2012).
- [84] S. Deng, L. Viola, and G. Ortiz, *Phys. Rev. Lett.* **108**, 036803 (2012).
- [85] J. Wang, Y. Xu, and S.-C. Zhang, *Phys. Rev. B* **90**, 054503 (2014).
- [86] F. Yang, C.-C. Liu, Y.-Z. Zhang, Y. Yao, and D.-H. Lee, *Phys. Rev. B* **91**, 134514 (2015).